Journal of Advanced Ceramics
2021, **10**(3): 565–577
https://doi.org/10.1007/s40145-021-0458-1

ISSN 2226-4108
CN 10-1154/TQ

Research Article

Crystal and electronic structure engineering of tin monoxide by external pressure

Kun LI[a,b], Junjie WANG[a,b,*], Vladislav A. BLATOV[c,b,d], Yutong GONG[a], Naoto UMEZAWA[e], Tomofumi TADA[f], Hideo HOSONO[f], Artem R. OGANOV[g,a,b,h]

[a]*State Key Laboratory of Solidification Processing*, *Northwestern Polytechnical University*, *Xi'an 710072*, *China*
[b]*International Center for Materials Discovery*, *School of Materials Science and Engineering*, *Northwestern Polytechnical University*, *Xi'an 710072*, *China*
[c]*Samara Center for Theoretical Materials Science* (*SCTMS*), *Samara State Technical University*, *Samara 443100*, *Russia*
[d]*Samara Center for Theoretical Materials Science* (*SCTMS*), *Samara University*, *Samara 443011*, *Russia*
[e]*Semiconductor R&D Center*, *Samsung Electronics*, *Gyeonggi-do 18448*, *Republic of Korea*
[f]*Materials Research Center for Element Strategy*, *Tokyo Institute of Technology*, *Kanagawa 226-8503*, *Japan*
[g]*Skolkovo Institute of Science and Technology*, *Moscow 143026*, *Russia*
[h]*Moscow Institute of Physics and Technology*, *Dolgoprudny 141700*, *Russia*

Received: December 14, 2020; Revised: January 7, 2021; Accepted: January 8, 2021

Abstract: Although tin monoxide (SnO) is an interesting compound due to its *p*-type conductivity, a widespread application of SnO has been limited by its narrow band gap of 0.7 eV. In this work, we theoretically investigate the structural and electronic properties of several SnO phases under high pressures through employing van der Waals (vdW) functionals. Our calculations reveal that a metastable SnO (β-SnO), which possesses space group $P2_1/c$ and a wide band gap of 1.9 eV, is more stable than α-SnO at pressures higher than 80 GPa. Moreover, a stable (space group $P2/c$) and a metastable (space group *Pnma*) phases of SnO appear at pressures higher than 120 GPa. Energy and topological analyses show that $P2/c$-SnO has a high possibility to directly transform to β-SnO at around 120 GPa. Our work also reveals that β-SnO is a necessary intermediate state between high-pressure phase *Pnma*-SnO and low-pressure phase α-SnO for the phase transition path *Pnma*-SnO →β-SnO → α-SnO. Two phase transition analyses indicate that there is a high possibility to synthesize β-SnO under high-pressure conditions and have it remain stable under normal pressure. Finally, our study reveals that the conductive property of β-SnO can be engineered in a low-pressure range (0–9 GPa) through a semiconductor-to-metal transition, while maintaining transparency in the visible light range.

Keywords: tin monoxide; van der Waals (vdW); topological relationship; phase transition; band gap

1 Introduction

The SnO of the space group *P*4/*nmm* is a *p*-type semiconductor with an indirect band gap (0.7 eV) [1] and shows promise as anode material in lithium rechargeable battery [1] and active layer of thin film transistors [2]. The bipolarity of SnO was first reported by experiments [3] and recently validated with theoretical calculations [4]. However, the narrow band

* Corresponding author.
E-mail: wang.junjie@nwpu.edu.cn

gap of SnO (~0.7 eV) hinders its extensive application in various related fields, e.g., solar cell [5]. To overcome this shortcoming, some efforts have been made including modifying the band gap of SnO and synthesizing a new SnO with a wider band gap. For instance, Peng *et al*. [5] proved that alloying with divalent cations (Mg, Ca, Sr, and Zn) could engineer the band structure of SnO to a suitable semiconductor for photovoltaics. Wang *et al*. [6] predicted a series of novel structures of mixed-valence tin oxides by combining density functional theory (DFT) calculations with the evolutionary algorithm USPEX (Universal Structure Predictor: Evolutionary Xtallography) [7–9]. Among these predicted structures, a novel phase of layered SnO with the space group $P2_1/c$ attracts us due to its excellent stability and interesting electronic properties at ambient pressure [6]. The new SnO phase is only 0.03 eV/atom, less stable than the most stable α-SnO phase at 0 GPa and is more stable than other previously reported SnO structures [6,10]. Furthermore, it was confirmed dynamically stable by phonon dispersion calculations and named as β-SnO [6]. Moreover, DFT calculations revealed that β-SnO has a band gap of around 1.7 eV, which is suitable for photo-functional applications [6]. However, no clear clue as to how such a new phase can be synthesized experimentally was provided. From perspective of crystallography, β-SnO can be regarded as a distortion of α-SnO and its space group $P2_1/c$ is a subgroup of the space group $P4/nmm$. Therefore, it may be expected that β-SnO can be obtained through a phase transition from α-SnO under specific condition, e.g., high pressure. In recent years, high-pressure synthesis has attracted extensive interest due to its various advantages such as synthesizing new materials with seemingly impossible structures and compositions at ambient pressure, e.g., $NaCl_3$ [11], KCl_3 [12], and Na_2He [13]. In fact, high-pressure study of α-SnO was performed experimentally once, but no high-pressure phase transition was observed in the conducting pressure range from 0 to 51 GPa [14]. Here, a systematic theoretical investigation was carried out to explore the possibility of obtaining β-SnO under high-pressure conditions up to 150 GPa. Previous study revealed that conventional local and semi-local density functionals in DFT cannot well deal with the structures of layered tin monoxides [6,15], which are bound by van der Waals (vdW) forces. The vdW correction within DFT has been validated as a useful way to improve the calculation for layered structures. Govaerts *et al*. [15] introduced different vdW functionals to rebuild the crystal structures and the electronic properties of α-SnO at 0 GPa, and observed that the optB86b functional [16] gave the closest lattice parameters to the experimental data. Allen *et al*. [4] proposed that the PBE0–vdW approach, with 15% Fock exchange, is also a good choice for calculation of both lattice parameters and electronic properties of α-SnO. However, a detailed test of available vdW functionals was still absent especially for the application at high pressures, which is necessary to the high-pressure simulation performed in our work.

In our study, we first tested all available vdW functionals to rebuild the crystal structures of α-SnO from 0 to 50 GPa using the result of available high-pressure experiment of α-SnO [14] as a reference. The tested vdW functionals include D2 and D3 corrections from Grimme *et al*. [17], Tkatchenko–Scheffler method [18], self-consistent screening in Tkatchenko–Scheffler method (TS–SCS) [19], many-body dispersion [19,20], SCAN–rVV10 functionals [21], and methods combined with hybrid functional HSE06 [22]. Among these tested functionals, HSE06–TS-SCS, a combination of HSE06 and TS-SCS, was suggested to be the best method under ambient pressure to calculate the crystal structure and electronic properties of α-SnO with high accuracy, while DFT-D3-BJ [23] shows a competitiveness under the high pressure. Furthermore, the phase transitions of SnO under high-pressure conditions (0–150 GPa) were carefully studied through employing the DFT-D3-BJ functional. The calculation suggests that α-SnO might transform to β-SnO at pressures higher than 80 GPa and two new phases of SnO with space groups $P2/c$ and $Pnma$ will appear at high pressures of 120–150 GPa. The possibility of synthesizing $P2/c$-SnO under high pressure and subsequently transforming to β-SnO upon the release of pressure is revealed. Moreover, energy, structure, and topological analysis revealed that both $P2/c$- and $Pnma$-SnO prefer to transfer to β-SnO when external pressure is released, suggesting that one could expect the formation of β-SnO via high-pressure synthesis from Sn and oxygen. The electronic properties of β-SnO under low external pressure (0–20 GPa) were studied using the DFT-D3-BJ functional. It is revealed that in a range of relatively low external pressures, the band gap of β-SnO can be continuously adjusted from 1.9 to almost 0 eV. Finally, we found that the conductivity and

optical transparency of β-SnO might be engineered by external pressure.

2 Computation methods

All DFT calculations in this study were conducted using the Vienna *ab initio* simulation package (VASP) [24]. Structure relaxation and electronic property calculation were performed through combining vdW correction and the Perdew–Burke–Ernzerhof (PBE) [25] functionals. The projector augmented wave (PAW) [26] potentials treating $5s^25p^24d^{10}$ and $2s^22p^4$ as valence electrons were used for Sn and O atoms, respectively. A plane-wave kinetic energy cutoff of 900 eV was set for all calculations. Monkhorst–Pack [27] Brillouin zone sampling grid with a resolution of $2\pi\times0.03$ Å^{-1} was used in structure relaxations, while a *k*-mesh with spacing of around $2\pi\times0.015$ Å^{-1} was applied in the electronic structure calculations. For the electronic structure calculation, our results were converged to within 10^{-4} eV/atom. For the structure relaxations, the simulation will stop until the force is converged to less than 0.001 eV/Å. Phonon dispersion calculations were carried out using the finite displacement method as implemented in the PHONOPY code [28]. Compared to other functionals, e.g., B3LYP [29], B3PW [30], and HSE06 [22], the PBE functional always provides a poor performance in the calculation of band gap of oxide materials [31,32]. Therefore, the Hartree–Fock mixing parameter and the screening parameter μ were respectively set to 25% and 0.2 Å^{-1} for the screened hybrid functional given by Heyd, Scuseria, and Ernzerhof (HSE06) adopted for accurate structure relaxation and electronic structure calculation in this work.

Standard PBE and HSE06 functionals do not give a good description of the layered SnO structures because the dispersion forces between layers cannot be properly accounted for. To overcome this problem, different corrections of DFT-D, vdW-DF, DFT-TS, DFT-D3-BJ and SCAN-rVV10 were tested [14,18,19,33,34]. DFT-D adds a correction term to a standard Kohn–Sham DFT result, which could be interpreted in the following form [23]:

$$E_{\text{disp}}^{\text{DFT-D}} = -\frac{1}{2}\sum_{\text{A}\neq\text{B}}\sum_{n=6,8,10,\ldots} s_n \frac{C_n^{\text{AB}}}{R_{\text{AB}}^n} f_{\text{damp}}\left(R_{\text{AB}}\right) \quad (1)$$

where the summations are over all atoms, C_n^{AB} denotes the *n*-th-order dispersion coefficient (orders n = 6, 8, 10, ...) between atoms A and B, and R_{AB} means the length of atom pair AB. The term s_n can be used to adjust the correction to the repulsive behavior of the chosen exchange–correlation density functional. The normal DFT-D3 method adopts zero-dumping function f_{damp}. As a result, $E_{\text{disp}}^{\text{DFT-D}}$ tends to be 0 while the R_{AB} approaches 0. Notably, the methods labelled "DFT-*" mean the combination of vdW functionals and the PBE functionals. Among these methods, the DFT-D3-BJ is built by introducing Becke–Jonson (BJ) damping to D3 method, leading to a constant contribution of $E_{\text{disp}}^{\text{DFT-D}}$ to total energy, which is more reasonable than zero-damping. In our work, DFT-D3-BJ correction shows a good performance of optimizing the structure of α-SnO in the whole pressure range, and subsequently is used to study the structural and electronic properties of β-SnO under external pressure.

Combined with structural relaxation using VASP code, USPEX has been proved as a successful tool to predict novel structures [6,11–13] and properties [35–37] especially at high pressures. Considering the high pressures we applied in the present study, USPEX is an ideal tool to search the globally stable phase of SnO at high pressures. In this work, three fixed-composition searches at pressure of 150 GPa were performed for SnO in unit cells containing 8, 12, and 16 atoms, respectively. The global optimization was carried out by USPEX to generate the potentially stable structures. All structures of the first generation were randomly produced and were optimized by DFT-D3-BJ using VASP to compare their enthalpies for the local optimization. 40% of the structures owing the lowest enthalpies in the first generation were used to generate next generation by variation operations including heredity (40%), lattice mutation (20%), trans-mutation (20%), and random generator (20%). The global and local optimizations are repeated alternately until the most stable structure was not changed for more than 8 or 16 generations.

Topological analysis for searching transition pathways among different SnO phases was performed using the program package ToposPro and the database of topological types (TTD collection) [38]. The RCSR three-letter symbols [39] and the symbols for derived nets [40] were used to designate the network topologies. The structures of all phases were represented as periodic nets and the transitions between different phases were considered as transformations between the nets. The network model of reconstructive phase transitions

(NMRT) [41] was applied to find the transition topological structures (subnets and supernets) between the initial and final phases. A subnet or a supernet can be obtained from a given periodic net by breaking existing bonds or creating new bonds, respectively. According to NMRT, if crystal structures A and B have different topologies, i.e., the corresponding periodic nets are not homeomorphic, then A and B cannot be transformed to each other without breaking and/or creating bonds. If A is a supernet of B, i.e., containing B, or vice versa A is a subnet of B, i.e., can be embedded into B, the transition A→B is direct and can be respectively performed by breaking or creating some bonds in A. In other cases, for example, when the coordination of atoms is the same in A and B, the transition passes through at least one intermediate net C, which is a common subnet (C1) or a common supernet (C2) of A and B. C1 consists of all bonds, which exist in both A and B, while C2 includes all bonds from A and B. Thus, to pass from A to B through C1, one should break those bonds in A, which do not exist in B, and then create new bonds, which exist in B, but not in A. Vice versa, to perform the transition through C2, one should perform these operation in an opposite order. That is why C1 and C2 form a pair of subnet/supernet, which characterizes the topological transformations during the transition. ToposPro enables one to find all common subnets and supernets of any nets and, hence, to reveal topological transformations of crystalline solids in an automated way.

The optical properties were obtained by combination of VASP and VASPKIT [42], while the absorption coefficient $I(\omega)$ was calculated by the following equation [43]:

$$I(\omega)=\sqrt{2}\omega\left[\sqrt{\varepsilon_1(\omega)^2+\varepsilon_2(\omega)^2}-\varepsilon_1(\omega)\right]^{\frac{1}{2}} \quad (2)$$

where $\varepsilon_1(\omega)$ and $\varepsilon_2(\omega)$ are the real and imaginary parts of the dielectric function, respectively. The VASPKIT was also used to calculate the wavefunction characters. In addition, the crystal orbital overlap populations (COOP) were examined by LOBSTER [44] to analyze the chemical bonds.

3 Results and discussion

3. 1 Comparison of vdW functionals

To verify the feasibility of vdW functional to layered SnO system, we first optimized the structure of α-SnO in the pressure range from 0 to 50 GPa in comparison with the available experimental data [14] (Table S1 in the Electronic Supplementary Material (ESM)). The calculated results from different functionals at 0, 10, 20, 30, 40, 50 GPa are shown in Fig. 1, Figs. S1–S5 in the ESM, and Tables S2–S7 in the ESM. Figure 1 shows that both PBE and HSE06 functionals overestimate the lattice parameter *c* dramatically at 0 GPa, whereas lattice parameter *a* can be well estimated, leading to a significant deviation of the *a*/*c* ratio and unit cell volume from experimental values. This result proved again that the lattice parameter *c* is drastically influenced by the interlayer vdW force. In addition, the revPBE and rPW86 functionals [45,46] are not suitable for relaxing α-SnO that the lattice parameters obtained from these two methods show huge error at each pressure.

As expected, the introduction of vdW corrections can greatly improve the calculation accuracy of lattice parameter *c* of α-SnO. The DFT-D2 and DFT-D3 functionals developed by Grimme *et al*. [17,34] give *c* values close to the experimental data while slightly overestimating the lattice parameter *a*. However, the DFT-TS functional developed by Alexardre and Matthias. [18] underestimates the lattice parameter *c* notably. Similar phenomena are observed in the calculations using MBD-202 and MBD-212 functionals, which considered many-body dispersion interactions among atoms [19]. The constant *a* calculated by the SCAN-rVV10 functionals developed by Peng *et al*. [21] shows a small error, but the lattice constant *c* is seriously underestimated. On the contrary, the DFT-TS-SCS functional developed by Alexardre *et al*. [19] can perfectly avoid the underestimation of the lattice parameter *c*, while a significant overestimation of the parameter *a* is observed. By combining the hybrid functional HSE06 and the vdW functional DFT-TS-SCS, the HSE06-TS-SCS functional can provide the best estimation of lattice parameters *a*, *c*, *a*/*c*, and volume for α-SnO at 0 GPa (Fig. 1). The estimated lattice parameters *a* and *c* at 0 GPa only slightly deviate from experimental values with errors of 0.08% and –0.62%, respectively. However, the lattice parameters yielded by HSE06-MBD-212 and HSE06-TS are worse than those obtained from HSE06-TS-SCS. It is noteworthy that the obtained structural parameters with the optB86b-vdW are the second best to HSE06-TS-SCS, which is in line with the previous studies [15].

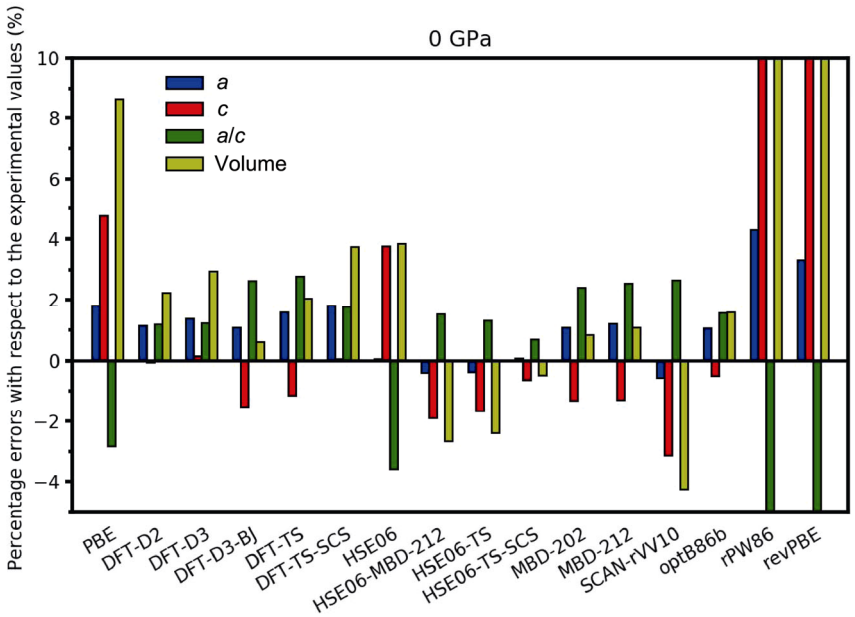

Fig. 1 Percentage errors of calculated *a* and *c*, *a*/*c* ratio, and volume of the unit cell of α-SnO using different functionals with respect to the experimental values at 0 GPa.

Although the deviation of calculated parameters from experimental values increases with the increase of external pressure (Figs. S1–S5 in the ESM), the HSE06-TS-SCS, DFT-D3-BJ, MBD-202, MBD-212, and optB86b functionals still exhibit their competitiveness, considering the good coherence between calculated lattice parameters and experimental values. Based on the results, we believe the HSE06-TS-SCS functional is the first choice to deal with Sn–O layered structures. However, in consideration of balancing calculation accuracy and cost under high pressures, we alternatively used the DFT-D3-BJ functional in the following calculations.

3. 2 Possibility of high-pressure synthesis

Figure 2 shows the crystal structures of α-SnO, β-SnO, *Pnma*-SnO, and *P*2/*c*-SnO. To compare the stabilities of α- and β-SnO at pressures from 0 to 150 GPa, the two structures were fully relaxed employing vdW functional DFT-D3-BJ (Fig. 3(a)). We found that the enthalpy of β-SnO becomes lower than that of α-SnO at pressures higher than 80 GPa, indicating that β-SnO is more stable than α-SnO at pressures higher than 80 GPa. Furthermore, to obtain the most stable SnO phase at high pressures, crystal structure searches for SnO were carried out using USPEX at 150 GPa. Two new phases of SnO with space groups *P*2/*c* and *Pnma* were identified. At 150 GPa,

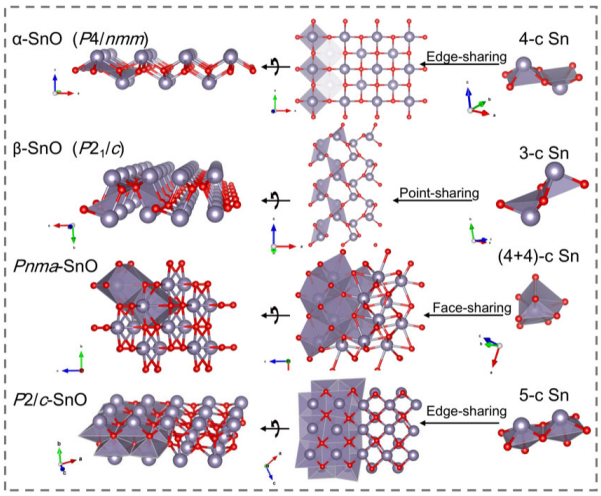

Fig. 2 Crystal structures of α-SnO, β-SnO, *Pnma*-SnO, and *P*2/*c*-SnO.

the calculated enthalpies of *P*2/*c*- and *Pnma*-SnO are 0.124 and 0.012 eV/atom lower than that of α-SnO, respectively (Fig. 3(a)).

The phonon calculations show that *P*2/*c*-SnO is dynamically stable in the pressure range of 120–150 GPa (Fig. S6 in the ESM). The imaginary frequencies were observed in the phonon calculations at 0–110 GPa for *P*2/*c*-SnO (Fig. S6 in the ESM), which suggests this phase will not be stable under ambient condition. Furthermore, the calculated enthalpy of *P*2/*c*-SnO is only 0.007 eV/atom lower than that of β-SnO ($P2_1/c$) at 120 GPa (where *P*2/*c*-SnO starts to be dynamically

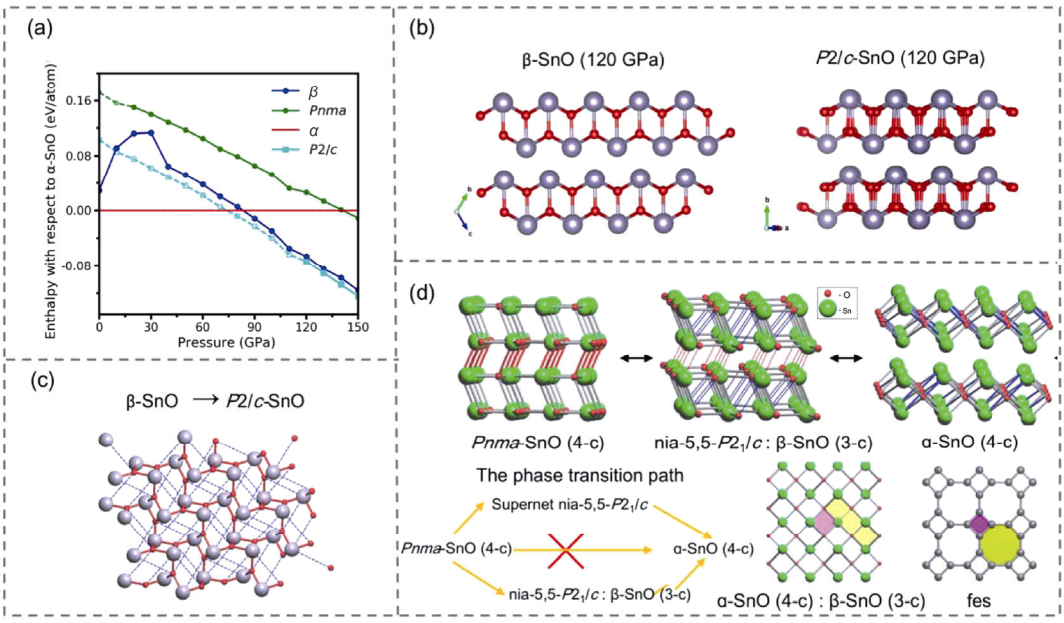

Fig. 3 (a) Enthalpy per atom for predicted tin monoxides as a function of external pressure with respect to α-SnO. For *Pnma*- and *P*2/*c*-SnO, the dashed lines and hollow symbols indicate the dynamical instability at certain pressure. (b) A schematic diagram to demonstrate the structural similarity between *P*2/*c*-SnO and β-SnO ($P2_1/c$). (c) Transformation of β-SnO ($P2_1/c$) to *P*2/*c*-SnO by forming new bonds shown by thin blue lines. (d) The phase transition from high-pressure *Pnma*-SnO to α-SnO through a supernet **nia**-5,5-$P2_1/c$ or β-SnO. Breaking the blue or red bonds in the supernet (upper middle of (d)) leads to α-SnO or *Pnma*-SnO, respectively, while breaking both types of bonds gives rise to β-SnO. Relation between *Pnma*-SnO and β-SnO layers: breaking thin red bonds in *Pnma*-SnO leads to the β-SnO **fes** topology. The idealized **fes** net consisting of 4- and 8-membered rings highlighted by magenta and yellow, respectively. These rings correspond to the rings of the same color in the bottom middle picture.

stable), while enthalpy of α-SnO is 0.073 eV/atom higher than that of *P*2/*c*-SnO (Fig. 3(a)). Figure 3(b) shows that the local structure of *P*2/*c*-SnO could be viewed as a slight deformation of that of β-SnO ($P2_1/c$). The topological analysis of the SnO crystal structures using ToposPro [38] indicates that these two structures belong to the same topology at high pressures. In the *P*2/*c*-SnO phase, all atoms are 5-coordinated, and thus two more Sn–O bonds are formed in β-SnO during the transition (Fig. 3(c)). The topology of the layers in the *P*2/*c*-SnO phase is known as 4^4Ia 2-periodic sphere packing [47], which has the maximum *P*4/*mmm* space-group symmetry. Both *P*2/*c* and $P2_1/c$ are general subgroups of *P*4/*mmm*, and the changes in symmetry are caused by a shift of the layers. Thus the β-SnO → *P*2/*c*-SnO or reversed *P*2/*c*-SnO →β-SnO transformations can be described as the topological reconstruction of each layer (Fig. 3(c)) followed by an appropriate shift of the layers. These results indicate the energy barrier of the phase transition at around 120 GPa from *P*2/*c*-SnO to β-SnO ($P2_1/c$) is much smaller than that to α-SnO. Therefore, it is highly expected that *P*2/*c*-SnO phase can be synthesized at high-pressure condition and may transform to β-SnO ($P2_1/c$) upon the release of external pressure at around 120 GPa.

Calculated phonon band structure shows that *Pnma*-SnO can be dynamically stable in the pressure range from 20 to 150 GPa (Fig. S6 in the ESM). The calculated enthalpy of *Pnma*-SnO is lower than that of α-SnO in the pressure range of 140–150 GPa but is always higher than that of *P*2/*c*-SnO, which suggests that *Pnma*-SnO is only a metastable phase in the studied pressure range. However, since the formation of compounds is often the interplay between thermodynamics and kinetics, the metastable *Pnma*-SnO may be synthesized by certain non-equilibrium experimental strategies. Therefore, the pressure-induced phase transition of *Pnma*-SnO was also hypothetically analyzed by topological method in this work.

It was revealed that the topological structures of α- and β-SnO belong to **sql** and **fes** topologies [40], respectively, while the topology of *Pnma*-SnO is **sra**. Schematic diagrams of **sql**, **fes**, and **sra** topologies (Fig. S7 in the ESM) and the details of topological analysis can be found in the ESM. It is known that in the transition state the subnet (low-coordinated structure) coexists

with the corresponding supernet (high-coordinated structure) because the stages of breaking and creating bonds can be reversed [41]. The corresponding supernet for the *Pnma*-SnO → α-SnO transition has the **nia**-5,5-$P2_1/c$ (derived from the NiAs type [48]) topology. This supernet contains all the SnO phases under consideration as its subnets; they can be obtained by breaking particular bonds in the supernet, thus elucidating the reconstructive phase transitions (Fig. 3(d)). Therefore, the following transition sequences can be proposed at decreasing pressure: *Pnma*-SnO (*Pnma*; **sra**)→ β-SnO ($P2_1/c$; **fes**) →α-SnO (*P*4/*nmm*; **sql**), i.e., the symmetry of the initial 4-coordinated *Pnma*-SnO decreases to $P2_1/c$, then some Sn–O bonds are broken yielding 3-coordinated β-SnO, and then some new Sn–O bonds are created giving rise to the 4-coordinated alpha phase (Fig. 3(d)). This transition reflects the easiest geometrical transformation: indeed, the bond that is broken in the **nia**-5,5-$P2_1/c$ transition state corresponding to one of the four weak bonds of the high-pressure *Pnma*-SnO.

Based on the above structure, topological, and enthalpy analysis, one can conclude that β-, *P*2/*c*-, and *Pnma*-SnO can be formed under high pressures and these new phases are likely to change or keep to β-SnO when the external pressure is removed. In addition, we believe the β-SnO will not transform to the α-SnO without external effects due to the dynamical stability of both phase and the small difference in enthalpy of formation between β-SnO and α-SnO at 0 GPa. Consequently, it is highly possible to synthesize β-SnO at high pressures and to keep it under ambient conditions.

In this section, we predicted a possible way for β-SnO synthesis, pressurization. The sequence of the phase transition of two stable high-pressure phases at 150 GPa to β-SnO and α-SnO are studied. The study shows the two different phases will preferentially transform to β-SnO when the pressure is released to 0 GPa. Therefore, it is suggested that the pressurization is a possible way for synthesis of β-SnO. Our work is a bold prediction of what may happen in the experiment based on the first-principle calculation and topological analysis. However, this work does not exclude the possibility of an unknown and stable structure under other pressures, which is complex and beyond this work.

3. 3 Electronic properties under external pressure

The previous phase transition analysis shows that external pressure can manipulate the structures of SnO in a wide range. To explore the application prospect of β-SnO, we investigated the influence of pressure on the electronic structure of β-SnO in the following section. At 0 GPa, the band structure calculated by HSE06-TS-SCS shows a direct band gap of 1.9 eV (Fig. S8 in the ESM). Due to the huge computational cost using HSE06-TS-SCS, the vdW functional DFT-D3-BJ is recommended in high-pressure study for its excellent estimation for lattice parameters of α-SnO in a wide pressure range. Indeed, the performance of DFT-D3-BJ functional on the electronic structure calculation of β-SnO is fairly good that it gives a band gap of 1.21 eV at 0 GPa, which is marginally narrower than that obtained by HSE06-TS-SCS. Although the PBE functional based methods may underestimate the band gap, the pressure-induced trend of electronic properties obtained by PBE functional based methods should be the same as that obtained by HSE06-TS-SCS. Therefore, the structures and electronic structures of β-SnO in the pressure range of 0–20 GPa were calculated using DFT-D3-BJ functional. The lattice parameters for the relaxed β-SnO are listed in Table S7 in the ESM.

The variation of calculated band gap of β-SnO as a function of external pressure is shown in Fig. 4(a). In the pressure range of 0–9 GPa, a linear reduction of the band gap with the increase of pressure can be observed and the band gap becomes almost zero at 9 GPa. With the further increase of external pressure, the band gap of β-SnO gets wider and then closes again at around 13 GPa (Fig. 4(a)). The calculated band structures of β-SnO along the k-path illustrated in Fig. 4(b) at 9 and 13 GPa are shown in Figs. 4(c) and 4(d) for a detailed study of this unusual band gap closing. Two band crossings near Fermi level can be observed in those calculated band structures, which indicates a semiconductor-to-metal transition of β-SnO under external pressure. In addition, it shows that the conduction band minimum (CBM) and valence band maximum (VBM) of β-SnO are shifted from the K line W–Γ to Γ–Y with the increase of pressure from 9 to 13 GPa. Then, the band gap of β-SnO gets open again (Fig. 4(a)) at pressures beyond 13 GPa. Finally, β-SnO becomes metallic at pressures above 50 GPa (Fig. S9 in the ESM). This pressure-induced variation of band gap indicates that the β-SnO might be used as a pressure sensor [49].

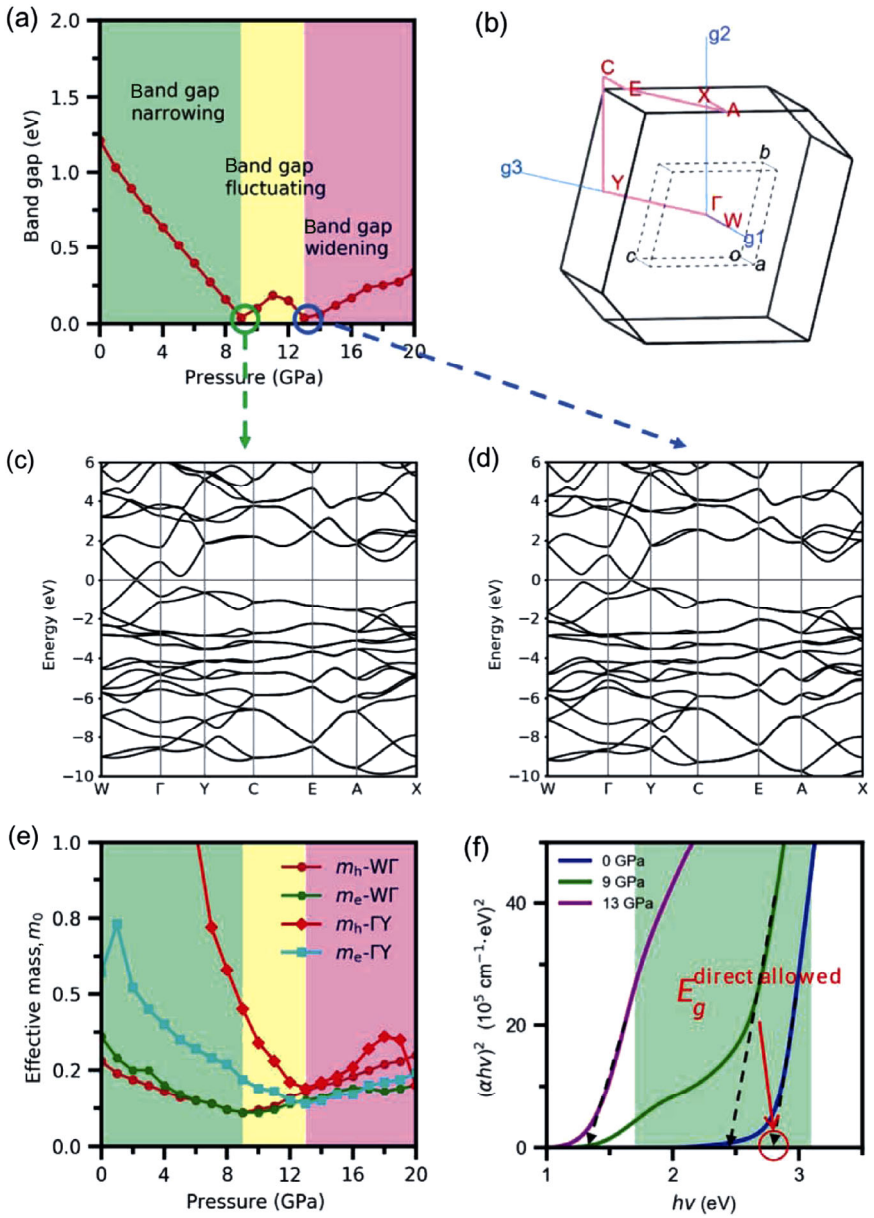

Fig. 4 (a) Variation of calculated band gap of β-SnO using DFT-D3-BJ functional as a function of external pressure in the range of 0–20 GPa. (b) The Brillouin zone of β-SnO. The calculated band structures at pressures of (c) 9 and (d) 13 GPa. (e) Calculated effective mass of β-SnO along different high-symmetry directions; m_h and m_e represent the effective mass of hole and electron, respectively. The m_h-WΓ means m_h along the W-Γ, etc. (f) Calculated absorption spectra, $(\alpha hv)^2$ vs. hv, for β-SnO at different pressures, where α and hv are the absorption coefficient and photon energy, respectively. The direct allowed band gap has been measured by extrapolating straight portion of the curves $(\alpha hv)^2$ vs. hv [50]. Notably, the edge of the absorption spectrum at different pressures were shifted +0.69 eV to fit the band gap estimated by the HSE06-TS-SCS. The green area represents the energy range of visible light.

The analysis of hole and electron effective mass demonstrates that pressure may alter the conductive property of β-SnO (Fig. 4(e)). It shows that all calculated effective mass along high-symmetry directions increase first and then decrease upon the increase of the external pressure. For instance, the m_h-WΓ (hole effective mass along the W–Γ direction) can be as small as $0.12m_0$ at 9 GPa. Moreover, the direct allowed band gap of the β-SnO is estimated to be around 2.8 eV at 0 GPa, which is similar to that of α-SnO (2.7 eV) [3] and *t*-ZrOS (2.5 eV) [51], implying the β-SnO could be a transparent semiconductor (Fig. 4(f)). A pressure-induced reduction of direct allowed band gap of the β-SnO can be also observed

(Fig. 4(f)). However, a significant direct allowed band gap (~2.4 eV) can be observed at 9 GPa. At the pressures higher than 13 GPa, the direct allowed band gap is smaller than the 1.7 eV, the lower boundary of the visible light area. Combined with previous analysis of hole and electron effective mass, we believe high conductivity and transparency could be obtained in the β-SnO at suitable pressures, such as 9 GPa.

It has been proved that the pressure-induced structural change can modulate the electronic properties of compounds [52,53]. Therefore, the variation of lattice constants (*a*, *b*, and *c*), distances of Sn–Sn pairs, and interlayer distance *d* in the pressure range 0–20 GPa were calculated by DFT-D3-BJ (Fig. 5) and used to explain the band gap change of β-SnO. As crystal axis *b* is not perpendicular to the plane of *ac*, $b\cdot\sin\alpha$ instead of *b* is shown in Fig. 5(a) (α is the angle between axis *b* and axis *c*). The distance between the Sn atoms of different layers was represented by the interlayer distance *d* (Fig. 5(b)). The distances of atom1–atom2, atom1–atom3, and atom1–atom4 (Figs. 5(c) and 5(d)) respectively give the first, the second, and the third nearest neighbor distances between Sn atoms on the same surface of the layer.

One can see that parameter *a* (Fig. 5(a)) and the distances of atom1–atom2 and atom1–atom4 (Figs. 5(c) and 5(d)) decrease monotonically over the entire pressure range, while *c*, $b\cdot\sin\alpha$ (Fig. 5(a)), interlayer distance *d* (Fig. 5(b)), and the distance of atom1–atom2 (Figs. 5(c) and 5(d)) show compression in the pressure range of band gap narrowing and then keep almost unchanged in the range of band gap fluctuating. In addition, the distance of atom1–atom3 show almost no compression under pressure. When the $b\cdot\sin\alpha$ and *d* become less compressible, the band gap starts to fluctuate. Therefore, it seems the compressions of parameter $b\cdot\sin\alpha$ (Fig. 5(a)) and interlayer distance *d* (Fig. 5(b)), which could affect the interlayer Sn–Sn interaction, have the strongest influence on the band gap change of β-SnO in the pressure range of band gap narrowing and fluctuating. Moreover, the opening of the band gap at the pressure that is higher than 13 GPa with the increase of parameter *c* (Fig. 5(a)) and the distance of atom1–atom3 (Fig. 5(d)) indicates that the in-layer interactions influence the band gap opening at high pressures.

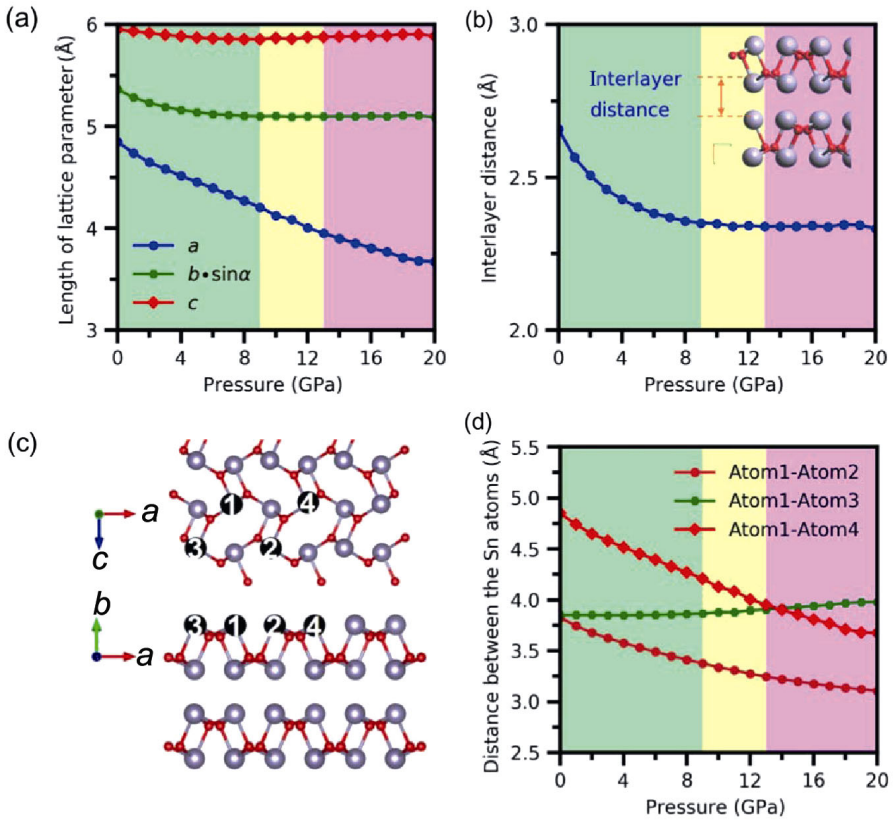

Fig. 5 Variation of (a) lattice parameters, (b) interlayer distance, and (c, d) distance between different Sn atoms on the same surface as a function of external pressure in the range of 0–20 GPa.

In order to gain insight into the relationship between the lattice deformation and band gap change of β-SnO, the decomposed band structure and COOP were examined and are shown in Fig. 6 and Fig. S10 in the ESM. One can see that O(p_z), Sn(s), and Sn(p) contribute more to the band structure near the Fermi level than other orbits (Fig. S10 in the ESM). Based on these calculation results, band diagrams were constructed and are shown in Fig. 6. It shows that the VBM and CBM of β-SnO are determined by both the interlayer Sn–Sn and intralayer Sn–O interactions. The vertical interactions Sn(s+p_z)–Sn(s+p_z) and Sn(p_x+p_y)–Sn(p_x+p_y) across the SnO layer consist of the antibonding states of VBM and bonding states of CBM, as shown in Fig. 6.

With the increase of external pressure in the range of band gap closing, Fig. 5 shows that the variation of geometric parameters $b\cdot\sin\alpha$ and interlayer distance d can directly influence the interlayer Sn–Sn distance and interaction. The continuous decrease of $b\cdot\sin\alpha$ and interlayer distance d is an indicator of the decreasing of Sn–Sn interlayer distance; therefore, the Sn–Sn interaction will be enhanced gradually (Fig. 5). The corresponding splitting in the energy between the bonding and antibonding levels of Sn(s+p_z)–Sn(s+p_z) and Sn(p_x+p_y)–Sn(p_x+p_y) interactions get enhanced, which leads to the narrowing of the band gap. Therefore, the decease of the interlayer distance and enhanced interlayer Sn–Sn interaction are responsible for the narrowing of band gap in the pressure range of 0–9 GPa. However, the oscillation and reopening (Fig. 4(a)) of the band gap with further increase in pressure cannot be explained by this mechanism.

As shown in Fig. S11 in the ESM, electron localization can be observed in the interlayer region, which corresponds to the Sn(s+p_z) states. With the increase of external pressure, it is expected that the pressure-induced decrease of interlayer distance of β-SnO will break the hybridization of Sn(s) and Sn(p_z) orbitals and force part electrons into the layer. The calculated decomposed band structures (Fig. S12 in the ESM) reveals the charge transfer from s to p_y orbital of Sn. Therefore, the intralayer Sn(p_x+p_y)–O(p) and Sn(s)–O(p) interactions would be enhanced and weakened, respectively. And both changes of intralayer effects would help open the band gap of β-SnO as illustrated in Fig. 6. In addition, the dehybridization of Sn(s) and Sn(p_z) orbitals would strengthen the stabilization effect of Sn(p_z) on the antibonding states of Sn(s)–O(p) interaction shown in Fig. 6 and helps to open the band gap as well. Therefore, the oscillation of

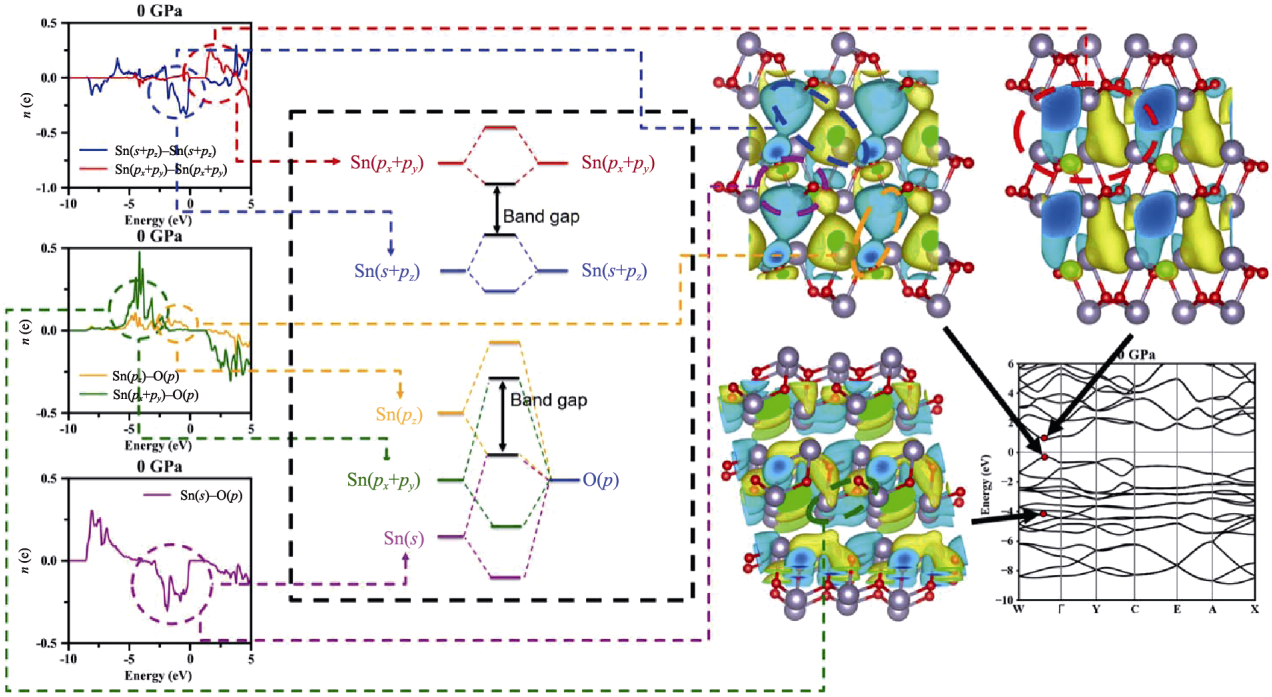

Fig. 6 Schematic diagram of orbital interactions, and the wave functions at representative points of the band structure for β-SnO at 0 GPa. In this work, axis z is perpendicular to the surface of SnO layer, while x and y are parallel to the axes a and c, respectively.

band gap in the pressure range of 9–13 GPa is the result of the competition of closing effect of interlayer Sn–Sn interaction and the opening effect of intralayer Sn–O interaction. With the further increase of external pressure, the intralayer Sn–O interaction became the dominant effect and opens the band gap continuously. This mechanism is evidenced by calculated wavefunction characters of CBM and VBM at different pressures (Fig. S13 in the ESM). The wave-function characters of VB–WΓ (VBM along the W–Γ) and CB–WΓ (CBM along the W–Γ) at 0 GPa reflect electron coupling between interlayer atoms, while the wave-function characters of VB–ΓY (VBM along the Γ–Y) and CB–ΓY (CBM along the Γ–Y) at 13 GPa trend to show the coupling of intralayer atoms.

4 Conclusions

We carried out a systematic theoretical study on the stability and electronic structure of SnO under external pressures. HSE06-TS-SCS and DFT-D3-BJ are respectively proved to be the best HSE- and PBE-based functionals for the relaxation of layered SnO. A phase transition from α-SnO to β-SnO is expected at around 80 GPa. Two high-pressure phases, *P*2/*c*- and *Pnma*-SnO, can be hopefully synthesized under high pressures and would transform to β-SnO after pressure releasing. Besides, the external pressure is demonstrated capable of modulating the band gap of β-SnO. A semiconductor-to-metal transition occurs in the low-pressure range of 0–9 GPa. In parallel with the pressure-induced variation of the band gap, the β-SnO is characterized by adjustable hole and electron mobilities. Moreover, β-SnO is expected to be a new transparent semiconductor at low pressures. Together, these results provide important implication that high conductivity and transparency of β-SnO could be obtained upon applied external pressure (such as 9 GPa). Finally, the mechanism behind variation of the band gap was proposed as the competition of interlayer Sn–Sn and intralayer Sn–O interactions. In summary, this work has been one of the first attempts to thoroughly examine the performance of vdW functionals under high pressures, which will guide the study of layered structures under high pressures. Moreover, this work demonstrates the mightiness of high pressures on structural modulation and new allotrope discovery of SnO, which would provide guidelines for the development of high effective materials in many structure-sensitive applications.

Electronic Supplementary Material

Supplementary material is available in the online version of this article at https://doi.org/10.1007/s40145-021-0458-1.

Acknowledgements

This work is supported by the National Natural Science Foundation of China (Grant No. 51872242) and the Fundamental Research Funds for the Central Universities (Grant No. D5000200142). Vladislav A. BLATOV thanks the Russian Science Foundation (Grant No. 16-13-10158) for support of developing the network topological model. Artem R. OGANOV thanks the Russian Science Foundation (Grant No. 19-72-30043).

References

[1] Idota Y, Kubota T, Matsufuji A, *et al.* Tin-based amorphous oxide: A high-capacity lithium-ion-storage material. *Science* 1997, **276**: 1395–1397.

[2] Ogo Y, Hiramatsu H, Nomura K, *et al.* P-channel thin-film transistor using p-type oxide semiconductor, SnO. *Appl Phys Lett* 2008, **93**: 032113.

[3] Hosono H, Ogo Y, Yanagi H, *et al.* Bipolar conduction in SnO thin films. *Electrochem Solid-State Lett* 2011, **14**: H13.

[4] Allen JP, Scanlon DO, Piper LFJ, *et al.* Understanding the defect chemistry of tin monoxide. *J Mater Chem C Mater* 2013, **1**: 8194–8208.

[5] Peng H, Bikowski A, Zakutayev A, *et al.* Pathway to oxide photovoltaics via band-structure engineering of SnO. *Appl Phys Lett Mater* 2016, **4**: 106103.

[6] Wang JJ, Umezawa N, Hosono H. Mixed valence tin oxides as novel van der Waals materials: Theoretical predictions and potential applications. *Adv Energy Mater* 2016, **6**: 1501190.

[7] Oganov AR, Glass CW. Crystal structure prediction using ab initio evolutionary techniques: Principles and applications. *J Chem Phys* 2006, **124**: 244704.

[8] Oganov AR, Lyakhov AO, Valle M. How evolutionary crystal structure prediction works—and why. *Acc Chem Res* 2011, **44**: 227–237.

[9] Lyakhov AO, Oganov AR, Stokes HT, *et al.* New developments in evolutionary structure prediction algorithm USPEX. *Comput Phys Commun* 2013, **184**: 1172–1182.

[10] Walsh A, Watson GW. Electronic structures of rocksalt, litharge, and herzenbergite SnO by density functional theory. *Phys Rev B* 2004, **70**: 235114.

[11] Zhang W, Oganov AR, Goncharov AF, *et al.* Unexpected stable stoichiometries of sodium chlorides. *Science* 2013, **342**: 1502–1505.

[12] Zhang W, Oganov AR, Zhu Q, *et al.* Stability of numerous novel potassium chlorides at high pressure. *Sci Rep* 2016, **6**: 26265.

[13] Dong X, Oganov AR, Goncharov AF, *et al.* A stable compound of helium and sodium at high pressure. *Nat Chem* 2017, **9**: 440–445.

[14] Giefers H, Porsch F, Wortmann G. Structural study of SnO at high pressure. *Physica B Condens Matter* 2006, **373**: 76–81.

[15] Govaerts K, Saniz R, Partoens B, *et al.* Van der Waals bonding and the quasiparticle band structure of SnO from first principles. *Phys Rev B* 2013, **87**: 235210.

[16] Klimeš J, Bowler DR, Michaelides A. Chemical accuracy for the van der Waals density functional. *J Phys: Condens Matter* 2009, **22**: 022201.

[17] Grimme S, Antony J, Ehrlich S, *et al.* A consistent and accurate ab initio parametrization of density functional dispersion correction (DFT-D) for the 94 elements H–Pu. *J Chem Phys* 2010, **132**: 154104.

[18] Alexandre T, Matthias S. Accurate molecular van der Waals interactions from ground-state electron density and free-atom reference data. *Phys Rev Lett* 2009, **102**: 073005.

[19] Alexandre T, Distasio RA, Roberto C, *et al.* Accurate and efficient method for many-body van der Waals interactions. *Phys Rev Lett* 2012, **108**: 236402.

[20] Alberto A, Reilly AM, Distasio RA, *et al.* Long-range correlation energy calculated from coupled atomic response functions. *J Chem Phys* 2014, **140**: 150901.

[21] Peng HW, Yang ZH, Perdew JP, *et al.* Versatile van der Waals density functional based on a meta-generalized gradient approximation. *Phys Rev X* 2016, **6**: 041005.

[22] Heyd J, Scuseria GE, Ernzerhof M. Hybrid functionals based on a screened Coulomb potential. *J Chem Phys* 2003, **118**: 8207.

[23] Grimme S, Ehrlich S, Goerigk L. Effect of the damping function in dispersion corrected density functional theory. *J Comput Chem* 2011, **32**: 1456–1465.

[24] Kresse G, Furthmüller J. Efficient iterative schemes for ab initio total-energy calculations using a plane-wave basis set. *Phys Rev B* 1996, **54**: 11169–11186.

[25] Perdew JP, Burke K, Ernzerhof M. Generalized gradient approximation made simple. *Phys Rev Lett* 1996, **77**: 3865–3868.

[26] Blöchl PE. Projector augmented-wave method. *Phys Rev B* 1994, **50**: 17953–17979.

[27] Monkhorst HJ, Pack JD. Special points for Brillouin-zone integrations. *Phys Rev B* 1976, **13**: 5188–5192.

[28] Togo A, Oba F, Tanaka I. First-principles calculations of the ferroelastic transition between rutile-type and $CaCl_2$-type SiO_2 at high pressures. *Phys Rev B* 2008, **78**: 134106.

[29] Becke AD. Density–functional thermochemistry. III. The role of exact exchange. *J Chem Phys* 1993, **98**: 5648–5652.

[30] Lee C, Yang W, Parr RG. Development of the Colle–Salvetti correlation-energy formula into a functional of the electron density. *Phys Rev B* 1988, **37**: 785–789.

[31] Eglitis RI, Popov AI. Systematic trends in (0 0 1) surface ab initio calculations of ABO_3 perovskites. *J Saudi Chem Soc* 2018, **22**: 459–468.

[32] Eglitis RI, Purans J, Gabrusenoks J, *et al.* Comparative ab initio calculations of ReO_3, $SrZrO_3$, $BaZrO_3$, $PbZrO_3$ and $CaZrO_3$ (001) surfaces. *Crystals* 2020, **10**: 745.

[33] Bučko T, Lebègue S, Gould T, *et al.* Many-body dispersion corrections for periodic systems: An efficient reciprocal space implementation. *J Phys: Condens Matter* 2016, **28**: 045201.

[34] Grimme S. Semiempirical GGA-type density functional constructed with a long-range dispersion correction. *J Comput Chem* 2006, **27**: 1787–1799.

[35] Lyakhov AO, Oganov AR. Evolutionary search for superhard materials: Methodology and applications to forms of carbon and TiO_2. *Phys Rev B* 2011, **84**: 092103.

[36] Yu SY, Jia XJ, Frapper G, *et al.* Pressure-driven formation and stabilization of superconductive chromium hydrides. *Sci Rep* 2015, **5**: 17764.

[37] Wang JJ, Hanzawa K, Hiramatsu H, *et al.* Exploration of stable strontium phosphide-based electrides: Theoretical structure prediction and experimental validation. *J Am Chem Soc* 2017, **139**: 15668–15680.

[38] Blatov VA, Shevchenko AP, Proserpio DM. Applied topological analysis of crystal structures with the program package ToposPro. *Cryst Growth Des* 2014, **14**: 3576–3586.

[39] Michael OK, Peskov MA, Ramsden SJ, *et al.* The Reticular Chemistry Structure Resource (RCSR) database of, and symbols for, crystal nets. *Acc Chem Res* 2008, **41**: 1782–1789.

[40] Blatov VA. Topological relations between three-dimensional periodic nets. I. Uninodal nets. *Acta Crystallogr A* 2007, **63**: 329–343.

[41] Blatov VA, Golov AA, Yang C, *et al.* Network topological model of reconstructive solid-state transformations. *Sci Rep* 2019, **9**: 6007.

[42] Wang V, Xu N, Liu JC, *et al.* VASPKIT: A pre- and post-processing program for VASP code. *Cond mat* 2019:1908.08269.

[43] Saha S, Sinha TP, Mookerjee A. Electronic structure, chemical bonding, and optical properties of paraelectric $BaTiO_3$. *Phys Rev B* 2000, **62**: 8828–8834.

[44] Maintz S, Deringer VL, Tchougreeff AL, *et al.* LOBSTER: A tool to extract chemical bonding from plane-wave based DFT. *J Comput Chem* 2016, **37**: 1030–1035.

[45] Dion M, Rydberg H, Schroder E, *et al.* Van der Waals density functional for general geometries. *Phys Rev Lett* 2004, **92**: 246401.

[46] Klimeš J, Bowler DR, Michaelides A. Van der Waals density functionals applied to solids. *Phys Rev B* 2011, **83**: 195131.

[47] Koch E, Fischer W. Types of sphere packings for

crystallographic point groups, rod groups and layer groups. *Z Kristallogr* 1978, **148**: 107–152.

[48] Blatov VA, Proserpio DM. Topological relations between three-periodic nets. II. Binodal nets. *Acta Cryst* 2009, **65**: 202–212.

[49] Shao G, Jiang JP, Jiang MJ, *et al.* Polymer-derived SiBCN ceramic pressure sensor with excellent sensing performance. *J Adv Ceram* 2020, **9**: 374–379.

[50] Tauc J. Optical properties and electronic structure of amorphous Ge and Si. *Mater Res Bull* 1968, **3**: 37–46.

[51] Arai T, Iimura S, Kim J, *et al.* Chemical design and example of transparent bipolar semiconductors. *J Am Chem Soc* 2017, **139**: 17175–17180.

[52] Wang F, Tan MP, Li C, *et al.* Unusual pressure-induced electronic structure evolution in organometal halide perovskite predicted from first-principles. *Org Electron* 2019, **67**: 89–94.

[53] Lu Y, Zhu SC, Huang E, *et al.* Pressure-driven band gap engineering in ion-conducting semiconductor silver orthophosphate. *J Mater Chem A* 2019, **7**: 4451–4458.